ICARUS **119,** 336–349 (1996)
ARTICLE NO. 0023

Titan's Surface, Revealed by HST Imaging

P. H. SMITH, M. T. LEMMON, AND R. D. LORENZ

Lunar and Planetary Laboratory, Department of Planetary Sciences, University of Arizona, Tucson, Arizona 85721
E-mail: psmith@lpl.arizona.edu

L. A. SROMOVSKY

Space Science and Engineering Center, University of Wisconsin, Madison, Wisconsin 53706

J. J. CALDWELL

Institute for Space and Terrestrial Science, Concord, Ontario

AND

M. D. ALLISON

NASA/Goddard Institute for Space Studies, 2880 Broadway, New York, New York 10025

Received June 15, 1995; revised September 1, 1995

We present for the first time relative albedo maps of Titan's surface. The maps were made from images taken by the Hubble Space Telescope's planetary camera (295 km per pixel) through atmospheric windows at 940 and 1080 nm. Coverage at all longitudes and between 45°S and 60°N was obtained with 14 orbits from 4–18 October 1994. Each image is characterized by haze with both limb effects (brightening) and a large north–south contrast. Subtracting an averaged image from each frame removes haze effects and reveals surface features of ~10% maximum contrast. Many features are clearly visible in multiple images and in both filters, but the surface map is dominated by a large, bright, roughly rectangular feature centered at 110°W, 10°S and elongated in an east–west direction (4000 × 2500 km^2): this feature and others indicate the diversity of Titan's surface. We consider the origin of the bright feature in an otherwise dark landscape and suggest that highland washing by methane rainfall is a likely mechanism. © 1996 Academic Press, Inc.

INTRODUCTION

Titan's surface has been considered "hidden" by its thick, haze-laden atmosphere following the Voyager 1 flyby. In the past 4 years, however, radar (Muhleman *et al.* 1990) and near-infrared (Lemmon *et al.* 1993, 1995, Griffith 1993) observations have penetrated the haze and have indicated that Titan's surface is heterogeneous. Ground based infrared adaptive optics studies (Saint-Pé *et al.* 1993) and a trial Hubble Space Telescope (HST) image with the wide field planetary camera (WF/PC; Smith and Lemmon 1993) indicated that it may be possible to resolve surface features. An earlier set of WF/PC images by Caldwell *et al.* (1992) measured the atmosphere's north–south asymmetry, but used filters that did not probe to the surface. In this paper we report a sequence of HST images taken with WF/PC-2, in wavelength bands covering windows of low opacity in Titan's atmosphere at 940 and 1080 nm: lower contrast images in the red continuum using the F673N filter are also discussed.

Our intent in this paper is to show the first maps of Titan's relative surface albedo at these wavelengths. Observable surface features on Titan are in themselves striking because of the large contribution of the overlying atmosphere. The surface features are discussed in the context of previous observations and theoretical work, but the scope of the paper does not extend to interpretation of the atmospheric effects, nor to using radiative transfer models to determine the reflectivity of the surface without atmospheric effects. No cloud features could be tracked at the 3σ level, although there are some subtle variations between image frames.

OBSERVATIONS

A sequence of observations of Titan was initiated on 4 October 1994 using HST's planetary camera, which has a pixel size of 0.046 arcsec that corresponds to ~295 km at the sub-earth point on Titan's disk (5150 km in diameter, Lindal *et al.* 1983). Our goals were twofold: to map the

0019-1035/96 $18.00
Copyright © 1996 by Academic Press, Inc.
All rights of reproduction in any form reserved.

TABLE I
Dates of the Observations, Longitudes of Central Meridian, and the Earth–Titan Distance for Each HST Orbit

Orbit	Date (UT)	LCM(°)[a]	Distance (AU)	Time step (hr)
0	10/4/94 14.2	124.4	8.8625	
1	10/4/94 19.9	129.8	8.8647	5.75
2	10/5/94 3.9	137.3	8.8678	8.00
3	10/5/94 10.4	143.4	8.8703	6.45
4	10/5/94 18.4	151.0	8.8734	8.05
5	10/6/94 1.3	157.4	8.8761	6.85
6	10/6/94 8.9	164.6	8.8791	7.65
7	10/7/94 22.0	199.6	8.8940	37.1
8	10/9/94 6.1	229.9	8.9072	32.1
9	10/10/94 12.8	258.7	8.9202	30.7
10	10/11/94 22.5	290.5	8.9349	33.8
11	10/13/94 5.1	319.4	8.9486	30.6
12	10/17/94 5.7	50.4	8.9938	96.5
13	10/18/94 13.8	80.6	9.0006	32.1

[a] LCM is in degrees (astronomical) east of the sub-Saturn point.

surface of Titan through the F850LP and F1042M filters and to measure cloud motions through red and methane-band filters.

Because wind velocities are only poorly estimated based on the observed temperature difference between the polar region and the equator (Flasar *et al.* 1981), we sampled velocities between -40 and $+50$ msec^{-1} as predicted for the lower troposphere, so that a feature would be seen at least 3 times before rotating off the visible disk. Fourteen HST orbits were specified with time gaps between the orbits to allow Titan to rotate. Time steps of 6–8 hr (about 6° rotation) were adopted for the first seven observations to search for clouds, increasing to about 32 hr for six of the last seven observations to achieve complete surface coverage. A gap of 96.5 hr between orbits 11 and 12 was necessitated by scheduling problems. Table I shows a complete list of all the orbital times, the longitudes of central meridian (LCMs), assuming synchronous rotation, and the time steps taken.

Within each orbit, images were taken through a number of filters (see Table II). The first orbit was used to study the north–south asymmetry of Titan, which is known to vary with time, presumably forced by seasonal variations (Sromovsky *et al.* 1981). The images taken at wavelengths below 650 nm are still being studied and will not be discussed in this paper. Another series of filters was chosen for its sensitivity to different altitudes above Titan's surface. These include the 673-nm continuum filter and the two methane filters at 619 and 889 nm. Finally, the filters that were thought to have the best chance of seeing to the surface were the F850LP (also expected to show clouds) and the F1042M filters, due to the decreasing optical thickness of Titan's haze with wavelength (see Lemmon 1994, Fig. 30). Filters were grouped into sets according to their science goals; these groupings are seen in the orbits column of Table II.

A standard calibration procedure was performed on each of the planetary camera images at the Space Telescope Institute. The background was subtracted and the best available flat fields were divided out. In addition, cosmic ray hits were manually replaced with local averages. The appearance of the F850LP and F1042M filter images revealed a strong contrast between the northern and southern haze with a pronounced limb brightening effect. Finding the subtle surface features within the overlying haze presented a challenge.

Several attempts were made to improve the contrast of the subtle features by deconvolving with the point spread function. These experiments introduced subtle artifacts at the few percent level and were subsequently abandoned. Titan is a small object, 0.8 arcsec in diameter: edge affects cannot be controlled, and deconvolution artifacts may be introduced. Therefore, all the results presented in this paper are from the calibrated, but undeconvolved, images.

Figure 1 shows the responsivity profile of both the F1042M and the F850LP filters along with the spectrum of the reflected light in normalized photon flux units. The product of the two curves gives the spectral distribution of the light sensed by the PC. Note that in the F850LP filter 40% of the light comes from the 940-nm window region while the F1042M filter 27% of the signal comes from the 1080-nm window (we define the windows as spectral regions where variations are seen in Titan's lightcurve—see Table III in Lemmon *et al.* 1995). As Lemmon *et al.* (1993) measured a variation of 8% in the 940-nm window and 12% in the 1080-nm window, we expect global variations on the level of about 1% within these two pass bands.

TABLE II
Exposure Times and Signal-to-Noise Ratios for the Different Filters, and the Orbits in which They Were Used

Filter	Central λ (nm)	Bandwidth (nm)	Exposure time (sec)	*S/N*	Orbits
F336W	332	37.1	160	119	0
F439W	430	46.4	40	175	0
F547M	548	48.7	7	199	0
F588N	589	4.9	40	190	0
F673N	673	4.7	40	183	0–6
F791W	779	130.4	3	195	0
F850LP	909	166.9	22	180	0–13
F1042M	1019	61.1	200	90	0, 7–13
F619, CH4	621	15.8	80	206	0–13
F889N, CH4	888	6.8	100	85	0, 7, 9, 11, 13

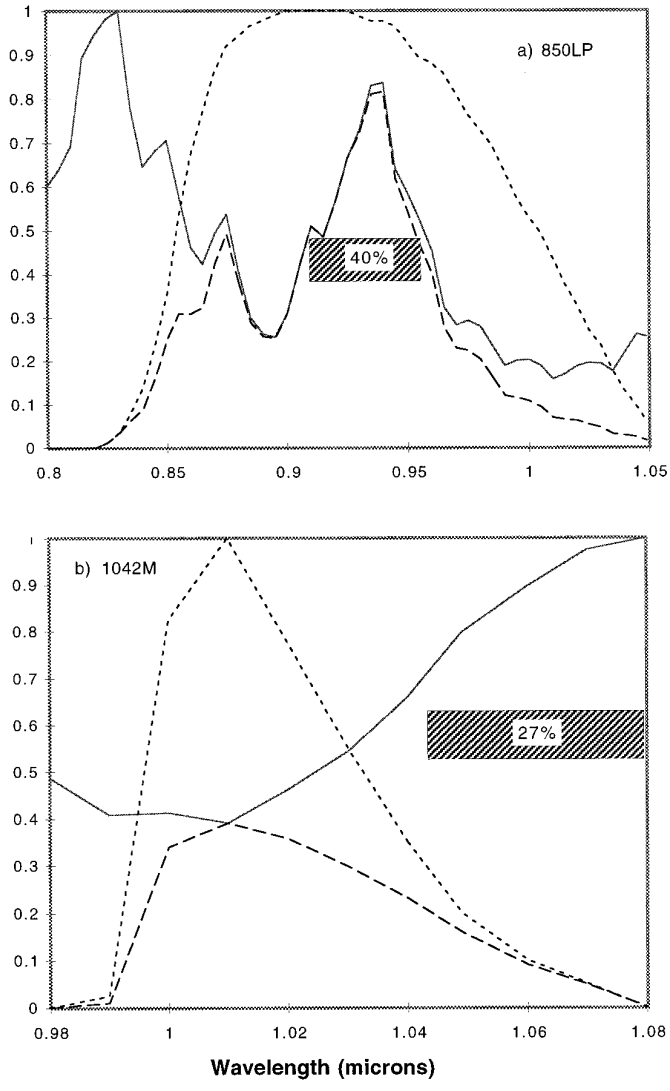

FIG. 1. Normalized light intensity reflected by Titan (solar flux multiplied by Titan's geometric albedo (Neff *et al.* 1984) as a function of wavelength, compared with the filter bandpass multiplied by the WF/PC-2 responsivity for the (a) F850LP and (b) F1042M filters. These show that they sample two distinct spectral regions sensitive to surface albedo. Solid lines refer to Titan's optical brightness (solar spectrum multiplied by Titan albedo); small dashes are the response of the telescope system (normalized detector sensitivity times filter transmission); long dashes show the product of Titan's spectrum and the instrument response. The hatched regions indicated the atmospheric windows (i.e., where albedo variations are seen in ground-based lightcurve monitoring—see Lemmon *et al.* 1995 Table III), and the percentages of light sensed through them is noted.

Surface Maps

Light in the methane continuum regions (940 and 1080 nm) within the bandpasses of the F850LP and F1042M filters probes to Titan's surface. Nevertheless, the surface is partially obscured by the haze, which has an optical thickness near unity at these wavelengths. Near the limbs the atmospheric path lengths are long, and the effects of the haze are particularly strong. This inhibits our ability to map the polar regions, which are always near the edge of the disk. Titan's atmosphere is in fact so extended that the outer pixel includes in its line of sight only the atmosphere, which has a perceptibly larger optical diameter (19.6 pixels) than Titan's surface diameter (17.6 pixels). In addition to the methane continuum, the bandpasses include methane absorption bands, in which all of the light comes from the atmosphere of Titan. Thus, the images contain both a surface component and an atmospheric component. The atmospheric component of the images shows limb brightening and a north–south asymmetry in the haze, which has a contrast of ~40% in each of the filters.

With signal to noise ratios on the order of 100 (see Table II), we can in principle observe surface features of a few percent contrast. In practice, such surface features can be identified only after we remove the atmospheric limb effects and haze asymmetry by subtracting the average of all images from each image. To put all images on the same scale and orientation, we rotate each image to a common orientation (north up) and expand each image to a common size—Titan's distance from Earth changed by 2% due to the Earth's motion about the Sun (see Table I), causing the apparent size of Titan to decrease with time. We then co-register the images, over-sampling the pixels (by bilinear interpolation) to avoid loss of information. For the 14 F850LP images, we use a weighted average: the first seven images viewed essentially the same face of Titan and were thus given reduced weight to avoid putting a surface feature in the average. A similar procedure, using an average made from only four images of Titan's darker and more featureless side, yields very similar results. The F1042M average image is a simple average of the eight original images, which were nearly equispaced in time. The effects of zonally symmetric surface features are retained in the averaging process as if they were atmospheric effects, and are lost in the subsequent subtraction process. The average F673N, F850LP, and F1042M images (Fig. 2) the limb effects and the haze asymmetry, but no surface features. Note that the haze asymmetry is much smaller in the F673N image than at longer wavelengths, and there is a marked change in the character of the limb effects.

We next subtract the average image from each of the original images for each filter. The resulting images show small scale features, but do not have atmospheric brightness features. Features near the limbs still have reduced contrast due to the larger atmospheric path length. For the F850LP images, the variation in the residual images is roughly ± 100 data numbers (DN), and the peak brightness of the average image is 2577 DN (7.7% total contrast). For the F1042M images, the variation in the residual images is roughly ± 80 DN, and the peak brightness of the average image is 1334 DN (12% total contrast). After subtracting

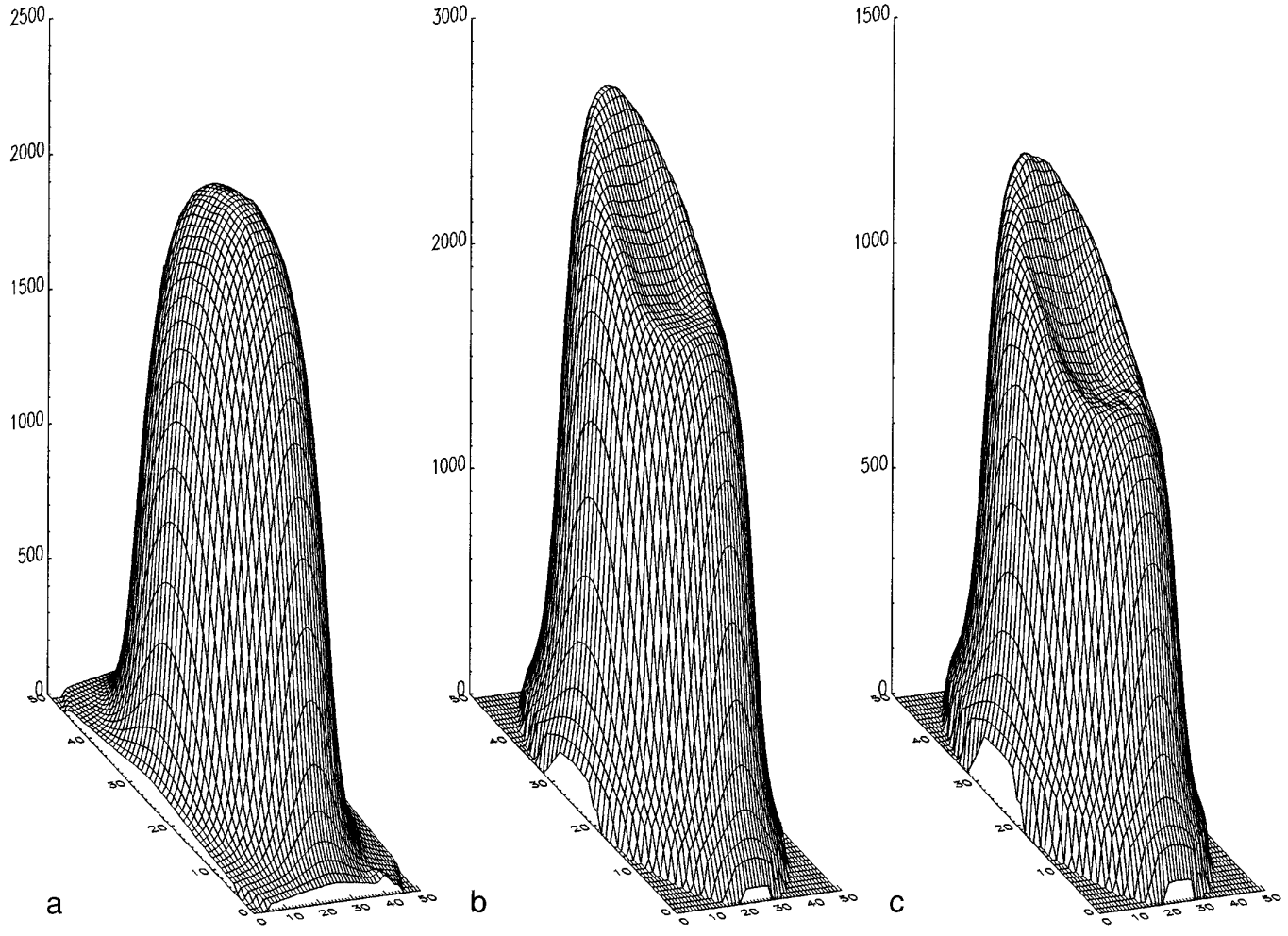

FIG. 2. Averaged images in the (a) F673N, (b) F850LP, and (c) F1042M filters. Although shown here resampled to 50 × 50 array elements, the images correspond to ~20 planetary camera pixels across. The vertical axes are in data numbers (DN). In (a), (b), and (c) the peak values of *I/F* are 0.329 (2238 DN), 0.184 (2577 DN), and 0.140 (1334 DN). Note the strong north–south asymmetry (the southern hemisphere is brighter in the season shown here, and is shown uppermost for clarity in these figures) in the F850LP and F1042M filters.

the average our effective signal to noise ratio for surface features becomes of order 10 in each difference image.

Each of the residual images is then projected onto a map, accounting for the viewing geometry at the time of the observation (assuming synchronous rotation and a surface radius of 2575 km). The map has a 3° × 3° latitude–longitude grid (61 × 120 pixels, including both poles) to provide a factor of two over-samplng of the planetary camera pixels near the center of the disk–the planetary camera pixels are 6° × 6° at the center of Titan's disk, and larger elsewhere on the disk. The Titan maps released at the 1994 Bethesda meeting of the AAS Division for Planetary Sciences (Smith *et al.* 1994) were made by simply averaging these projections (for each map pixel, we weighted images with the map pixel near the center of the disk more than those with the map pixel near the edge of the disk).

The maps we present here use a more refined method (they are available on the internet at http://www.lpl.arizona.edu/~lemmon/titan/titan.html). Plotting intensity against emission angle shows a variation between images (Fig. 3) of approximately μ^2 (where μ is the cosine of the titanocentric angle between the point of interest and the observer). Formally there is no reason to expect the residual images to follow this μ^2 law, although features are better observed near the center-of-disk due to geometric effects ($\sim\mu^1$) and atmospheric extinction effects are related to μ^1 for an optically thin atmosphere. Varying the exponent or the form of the relation introduces additional degrees of freedom without significant improvement to the fit: we adopt μ^2 for its simplicity and because it satisfies our needs. Figure 3 indicates the estimated intensities, relative to the average image, that would be seen if these

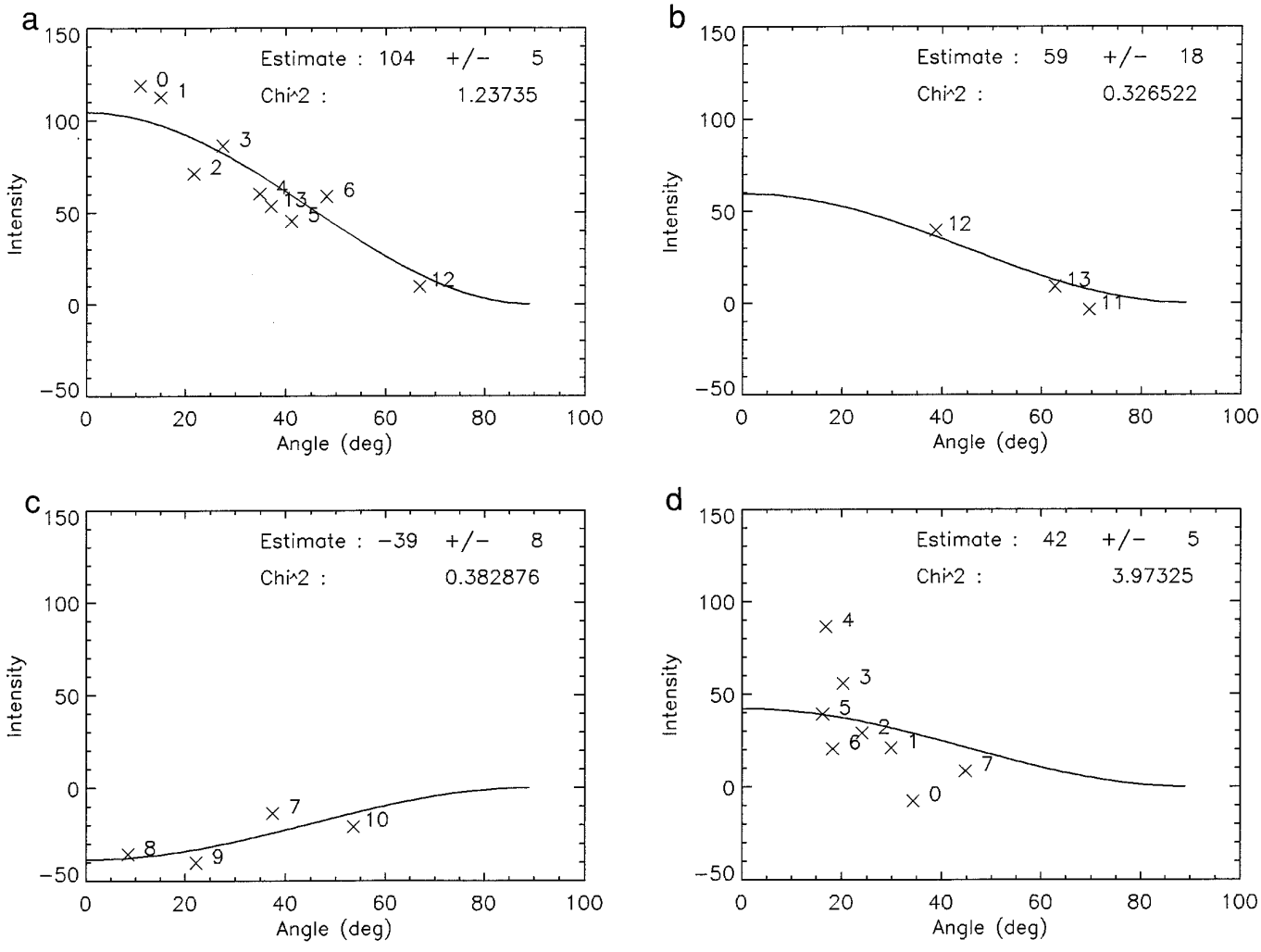

FIG. 3. Feature contrast (intensity relative to average image) as a function of angular distance from the sub-telescope point (crosses, with corresponding image number—see Table I), and best μ^{-2} fit (line). Panel (a) corresponds to the center of the bright feature, (b) is the smaller, bright region suggested by ground-based observations, (c) is a typical dark region, and (d) is the center of the "spit" at the north end of the bright region, with a large scatter in the data. Letters correspond to the locations shown on the map in Fig. 8. In 3(e), data shown are points in images between 30°N and 30°S, for I_0 values between −50 and −60 DN (crosses) and 100 and 110 DN (diamonds), renormalized to I_0 values of −50 and 100, respectively. Lines show μ^2 law for these I_0 values: the data follow the law well, and there is excellent discrimination between the two cases shown, except near the limb. A change in μ^2 of 0.1 corresponds to ~1 planetary camera pixel.

regions were at the sub-telescope point ($\mu = 1$). For each position on the map i, the estimate minimizes the reduced χ^2, which can be written as

$$(\chi^2)_{v,i} = \frac{\sum_j (I_{0,i}\mu_{ij}^2 - I_{ij})^2 \sigma^{-2}}{(N-1)}, \tag{1}$$

where $I_{0,i}$ denotes the estimated $\mu = 1$ intensity for location i, μ_{ij} is the cosine of the angle between the sub-telescope point and the area (i) of interest on image j, which appears in the image with brightness I_{ij} and uncertainty σ. At minimum χ^2, our estimate reduces to

$$I_{0,i} = \frac{\sum_j I_{ij}\mu_{ij}^2}{\sum_j \mu_{ij}^4}, \tag{2}$$

where the summation is done over each image (j) in which the location (i) appears. Figure 4 shows the maps at three wavelengths generated using the estimation technique described above; a color table is assigned to the values of I_0 and contrast contours are shown every 2%. By astronomical convention east is to the left of north, but this is not well-suited to discussions of maps, in which east is expected to the right of north. We will use cartographic convention,

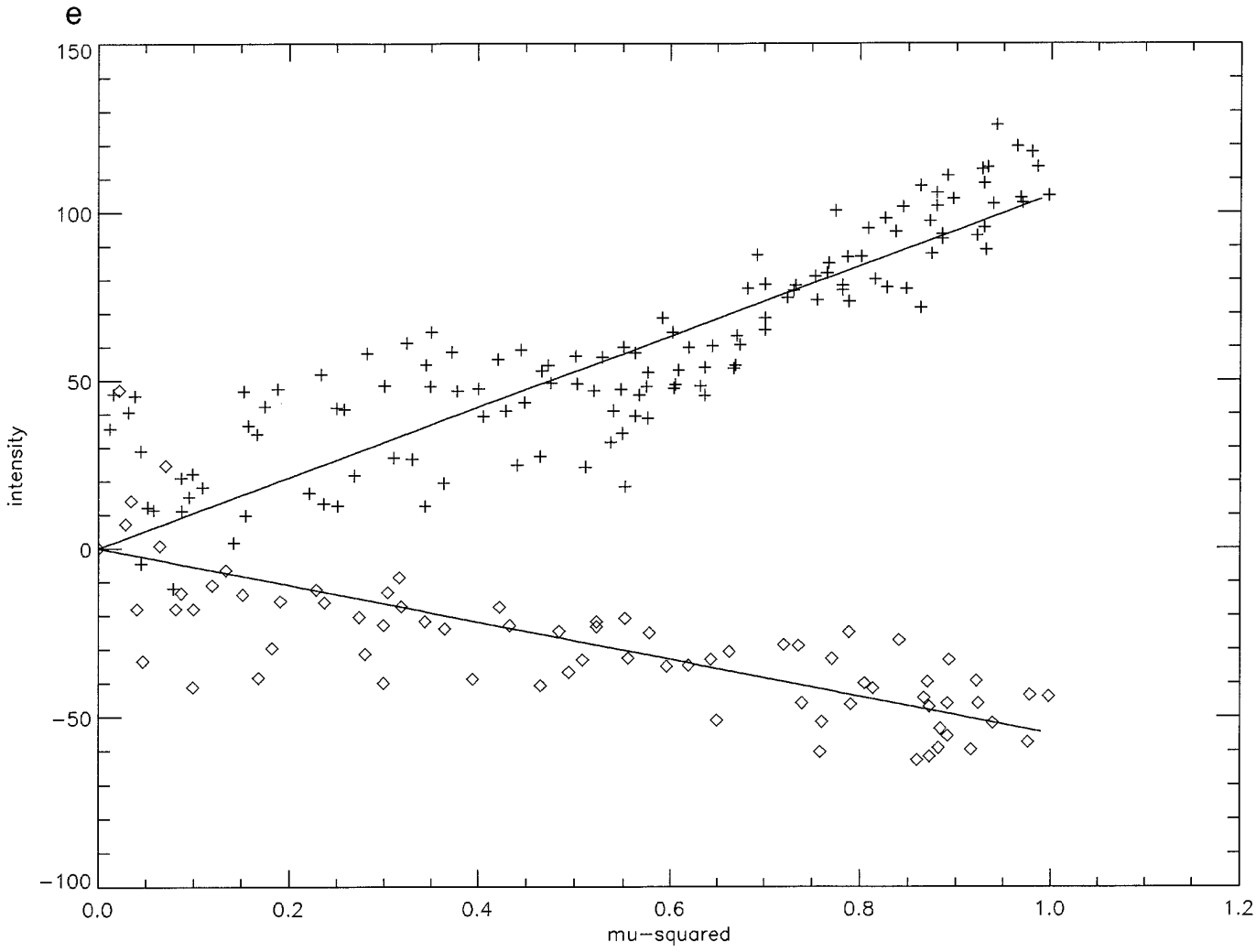

FIG. 3.—*Continued*

reserving astronomical convention for the discussion of Titan's orbital position (e.g., in Table I). The solid gray color at the north and south borders of the maps and extending toward the equator near 0° longitude (also near 170°W longitude in the F1042M map and covering most of the F673N map) represents areas that were not imaged or were only seen at the limb. Note that the maps are centered on the anti-Saturn point (180°E, 0°N).

For the F850LP map, σ is estimated to be 14 DN, and the RMS error of the map fit is 15 DN. The uncertainty in our estimation of $I_{0,i}$ is

$$\sigma_{I_{0,i}} = \frac{\sigma}{\sqrt{\sum_j \mu_{ij}^4}}. \quad (3)$$

On the F850LP map, these uncertainties range from 6 DN (3% of the total variation on the map) in the well sampled western side of the bright region, to near 14 DN in the equatorial part of the dark area, to very high values near the poles. In the 10°W coverage gap, the uncertainties are all larger than 21 DN (11% of the total variation on the map). Figure 5 shows maps of the uncertainty in I_0. These clearly show the decreased uncertainty in the region where we had the best coverage, as well as showing the coverage gaps at 10°W (F850LP and F1042M) and at 160°W (F1042M only).

For the F673N images, the level of variation in the residual images is consistent with the expected noise, although the brighter pixels are clustered in the region of the bright feature seen at longer wavelengths. The optical depth at normal incidence of the haze is about 3 at this wavelength, so light has little probability of being reflected by the surface and reaching the viewer without multiple scatterings in the atmosphere. The F673N map is included because, while the contrast is low relative to the noise, the shape and location of the bright region bears a striking similarity to the F850LP map. There is good agreement between the

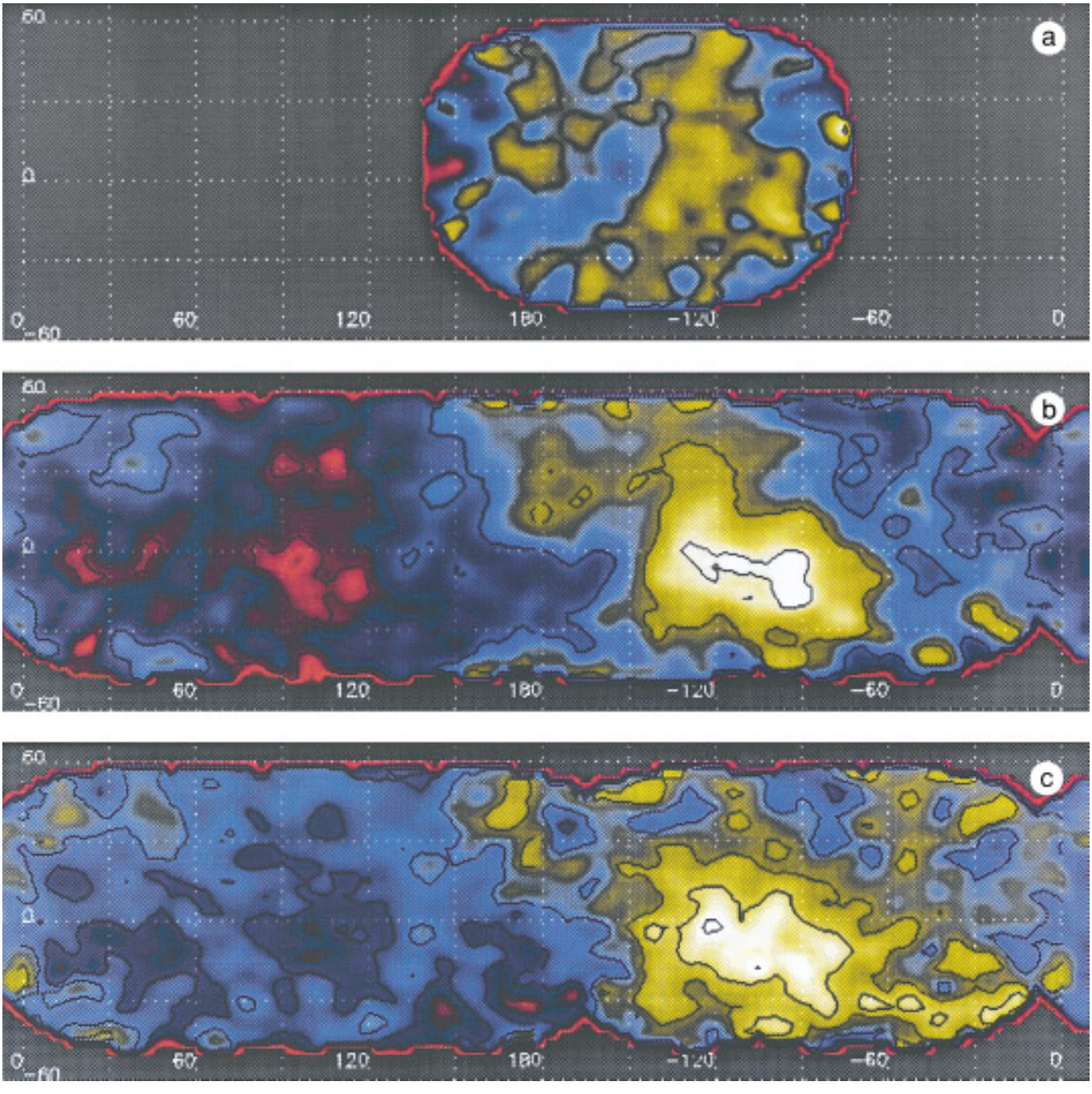

FIG. 4. Maps of Titan's surface generated from the HST observations using the methods described in the text. The projection is cylindrical, and grid labels are omitted for clarity: the grid spacing is 30°, with the anti-Saturn point (180°E, 0°N) at the center (for reference the leading face is centered at 90°W). Maps are shown for (a) F673N, (b) F850LP, (c) F1042M filters, with the color scale red (dark)–blue–yellow (bright). Contours are shown every 2% of the maximum *I/F* in the average image. Fig. 4d shows a zonal cut of contrast (map intensity averaged over latitudes ±6°/peak intensity of the raw images) through the maps at the three wavelengths (Solid line, F850LP; Dashed line, F1042M; Dotted line, F673N) with the associated color scale for the F850LP map (each map is stretched to fill the color scale: overall map contrasts are similar to the curves shown here). Note the characteristic saddled peak at all three wavelengths.

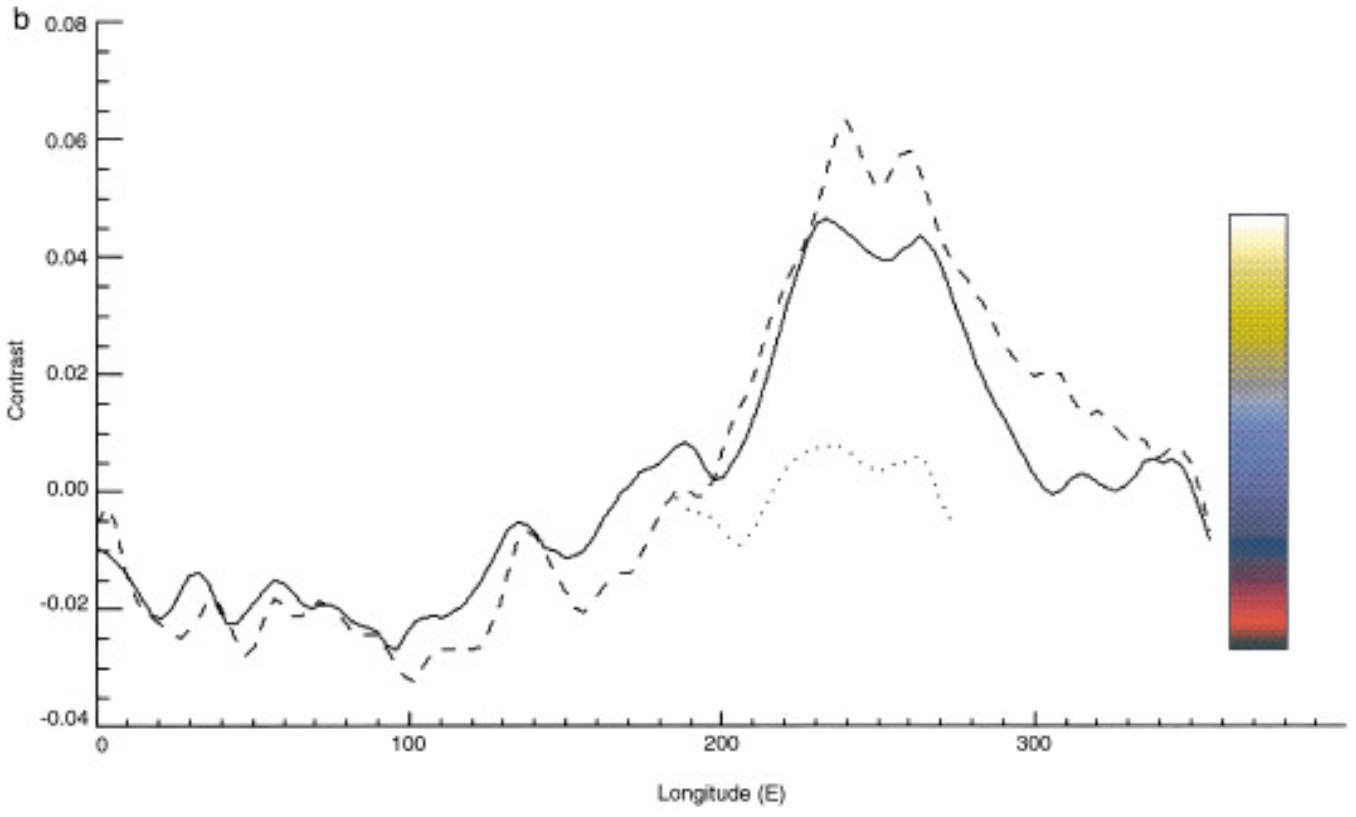

FIG. 4.—*Continued*

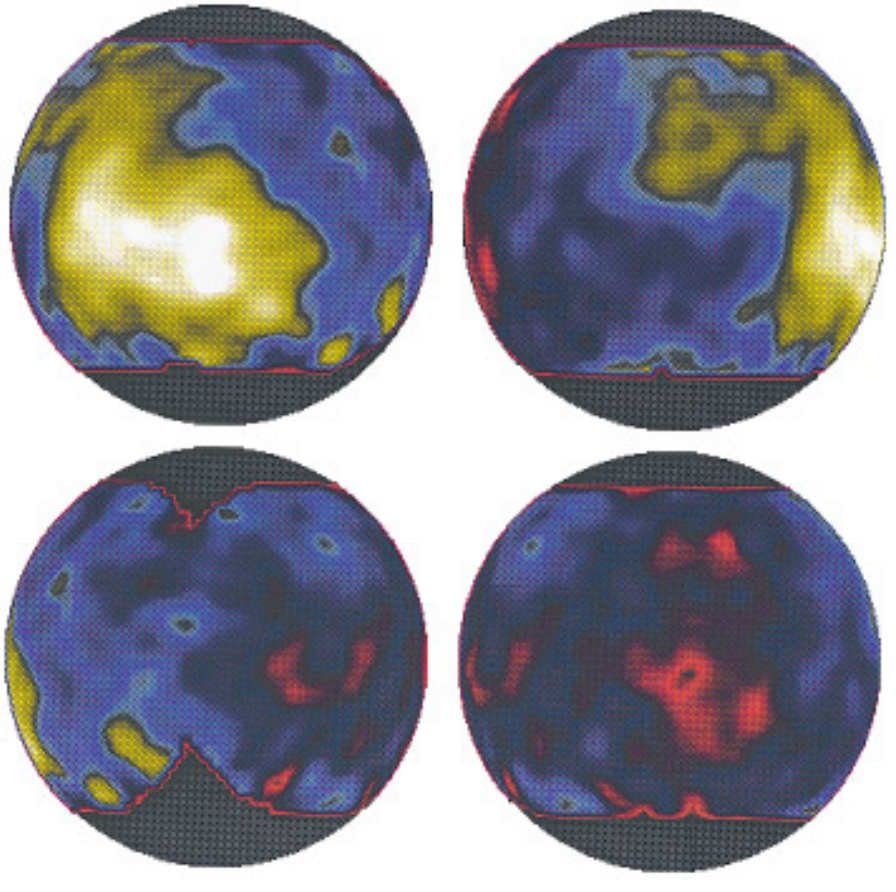

FIG. 6. F850LP map in orthographic projection. The faces visible are the leading hemisphere, the anti-Saturn hemisphere, the trailing hemisphere, and the Saturn-facing hemisphere, clockwise, from upper left.

bright locations seen in the three different filters. Additionally, a zonal cut through the map (Fig. 4d), averaging the brightness of a band $\pm 6°$ about the equator, yields a characteristic saddled peak at all three wavelengths at the same longitude.

The features have been further verified by comparing maps made using independent subsets of F850LP images: for example, two maps, one made from even-numbered orbits and one made from odd-numbered orbits, are highly correlated. Further, the large bright feature can be tracked from one image to the next, verifying that it co-rotates with the surface. However, smaller features ($\sim\frac{1}{5}$ the grid spacing on the map), features with small contrast, and features near the edges are questionable. We have inspected a map made without including images containing the bright feature in the original average image; the distribution of features in the dark area is not changed, indicating that these features are not inverse features due to the bright spot and are not due to noise in the average images.

The most striking feature in the maps is the large bright feature near (110°W, 10°S) covering some $4000 \times 2500\ \text{km}^2$. The western side of this feature is in the region of the best coverage for the F850LP map. The extension to the northwest of the main feature is real, as is the darker gap between the extension and the main part of the bright feature. The connection between the two may not be real—this region, shown in Fig. 8 as region D has an anomolously poor fit, as the scatter of the data is large (see Fig. 3d), perhaps due to cloud motions or cosmic ray hits on the detector. Conversely, we have a better view of the eastern side in the F1042M map. We have closely examined the map for features other than the large bright area. Specifically, the bright spots at 10°W, 25°S and at 50°W, 20°N have brightnesses approximately 2-sigma above the background and are larger in size than a single planetary camera pixel. Additionally, the two darkest regions, shown in red, at 100°E, 10°S and at 110°E, 30°N, and the bright region at 40°E, 40°N, have a similar contrast level and are larger still. Each of these spots appears in multiple images and in the F850LP and F1042M maps. Thus, although most of the following discussion is restricted to the large bright region, the rest of Titan's surface has contrast variations that appear to be real.

In order to find clouds in the troposphere, we have also examined the difference images for features that moved relative to the map grid. There are no easily identifiable and trackable clouds in the images. Any widespread clouds are either uniformly distributed (at our ~295-km coarse-graining), zonally distributed (in which case the average-image subtraction would have removed them), or optically thin.

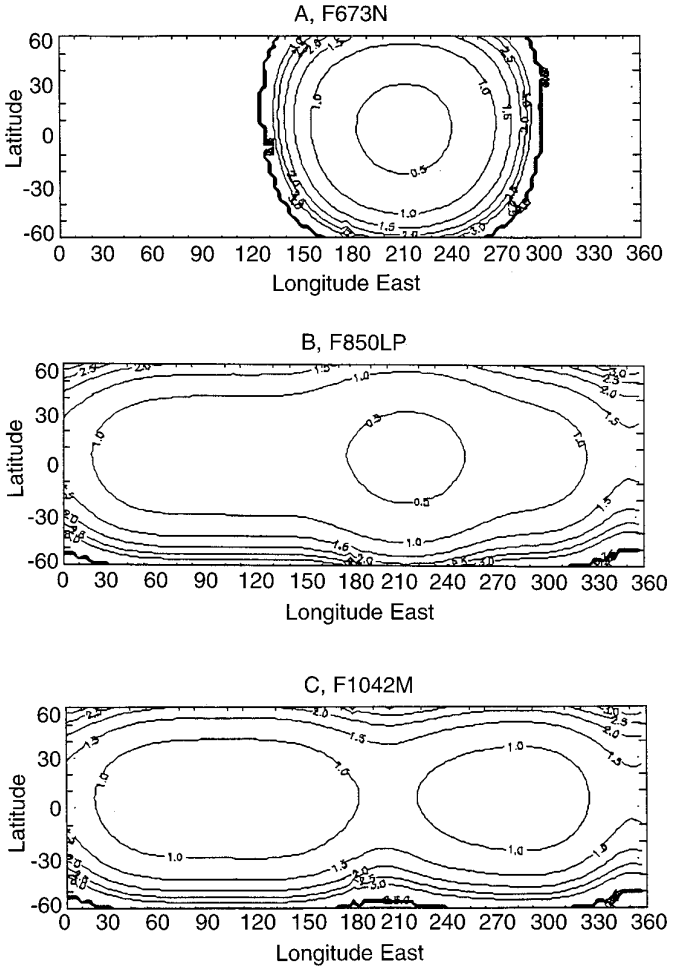

FIG. 5. Uncertainties for relative albedo maps. Contours in $\sigma_{I_{0,i}}/\sigma$ of 0.5, 1.0, 1.5, 2.0, and 2.5 are shown for the (A) F673N, (B) F850LP, (C) F1042M maps (Fig. 4). Equation (3) gives the relationship between σ (the uncertainty in the difference images) and $\sigma_{I_{0,i}}$ (the uncertainty in the relative albedo map).

DISCUSSION

Comparison with Ground-Based Data

Titan's lightcurve in the near-infrared is well established. The data set with the most complete global coverage is the 2-μm lightcurve of Lemmon *et al.* (1995). In the 2-μm window, the haze is optically thin, so atmospheric effects such as limb effects are smaller and the surface is more easily observable—in fact the lightcurve amplitude is 30%. Lightcurves at shorter wavelength methane windows (including the 940-nm window) have a shape consistent with the 2-μm lightcurve, but worse coverage; we will compare our data to the 2-μm lightcurve. For easy visual comparison with the ground based data sets, Fig. 6 shows orthographic projections of the F850LP map as it would be seen in four orbital positions: (clockwise from upper left) greatest eastern elongation, inferior conjunction, greatest western elongation, and superior conjunction.

As atmospheric effects are much less important in the 2-μm window than at 940 and 1080 nm, we calculate a map-based lightcurve without a thick atmosphere obscuring the

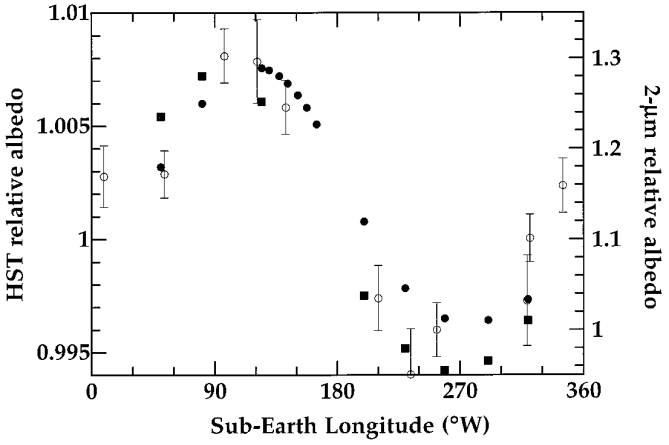

FIG. 7. Light curves of Titan, derived from the HST maps, compared with that from ground-based observations. Filled symbols correspond to a lightcurve generated by appropriately sampling our map (F850LP, filled circles; F1042M, squares) and open circles represent a lightcurve from ground-based spectroscopy at 2 μm.

surface features. To obtain a map-based lightcurve, for each of the image orientations we integrate over the map for the relative albedo. This is done for LCMs corresponding to those of each of the images. We then compare the integrals with the disk-integrated *I/F* for the average image at each wavelength (which is approximately the geometric albedo). Figure 7 shows the lightcurves derived from the maps compared to the Lemmon *et al.* (1995) lightcurve. The ground-based observations have consistently shown a leading-face bright region in 1975 (Fink and Larson 1979), 1978 (Cruikshank and Morgan 1980), 1989 and 1990 (Griffith 1993), 1992 (Lemmon *et al.* 1993), and 1993 (Lemmon *et al.* 1995). We identify the large feature in the map as the bright spot observed from the ground at longer wavelengths, and this suggests that the feature is persistent.

Figure 8 shows that the large, bright feature also appears coincident with the radar "bright spot" identified by Muhleman *et al.* (1990, 1995). A second bright region at 10°W, 25°S is at the longitude where ground-based near-infrared lightcurve monitoring (Lemmon *et al.* 1995) has suggested a possible, smaller bright spot. Although this spot appears in only two images (and only at the edge in one of these—this region is at the edge of the coverage gap), it is among the best candidates to be a real feature away from the main bright region. The longitudes of the Lemmon *et al.* (1995) bright spots are shown superimposed on the map in Fig. 8.

Rotation Rate

Historically, Titan has been assumed to be in a state of synchronous rotation. However, observations of a radar bright spot by Muhleman *et al.* (1995) suggested that Titan might instead have a slightly supersynchronous rotation i.e., a period of 15.911 days, as against the orbital period of 15.945 days. The plausibility of this was verified by Sears *et al.* (1994) who found that if there was no mass asymmetry (bulge) large enough to capture Titan into synchronous tidal lock, such a supersynchronous rotation state is allowed, given Titan's eccentric ($e = 0.029$) orbit. Lemmon *et al.* (1995) were able to show, using only their data from 1992 and 1993, that Titan's rotation period could be constrained to 15.95 ± 0.025 days. Including a 1975 observation by Fink and Larson (1979), Lemmon *et al.* (1995) showed that the rotation period must be 15.949 ± 0.006 days, a figure compatible with synchronous rotation, but not with the period determined by radar.

We have examined the images reported in this paper to measure the rotation period, attempting to match the edge of the bright feature in different images. The bright region shown in the map appears in the first five images in the sequence of F850LP images and in the last two. The angular dependence in Fig. 3 and the maps in Fig. 4 were generated assuming synchronous rotation. For the 14-day time baseline and a position determination accuracy of ± 1 map pixel (=0.5 planetary camera pixels at the equator, or $\sim 3°$ longitude) the rotation of the large bright feature could be constrained to between 15.815 and 16.075 days, a range that includes the radar period, and synchronous rotation: edge detection is difficult, however, as limb effects are significant. The 14-day timebase is inadequate to make better constraints on the rotation period than are presently offered by 20 years of ground-based observations. We plan to conduct further HST imaging of Titan, reimaging the bright region. The additional data will allow the period to be constrained to about 1 part in 1000, or of the same order as the lightcurve fitting by Lemmon *et al.* (1995).

The Nature of the Features

With knowledge of the location and shape of surface features, we can begin to investigate their nature. In the following we consider two distinct hypotheses to explain the appearance of the large, bright feature:

1. The "nominal" surface is dark, but an impact event has excavated fresher, brighter material from below the surface, or ammonia–water volcanism has emplaced a recent bright feature over the underlying darker terrain.
2. Meteorological processes have cleansed dark material from elevated or mountainous terrain, exposing brighter material beneath.

Our assumption for both hypotheses is that the bright material is water ice, and the dark material is probably organic. These hypotheses are the most consistent with

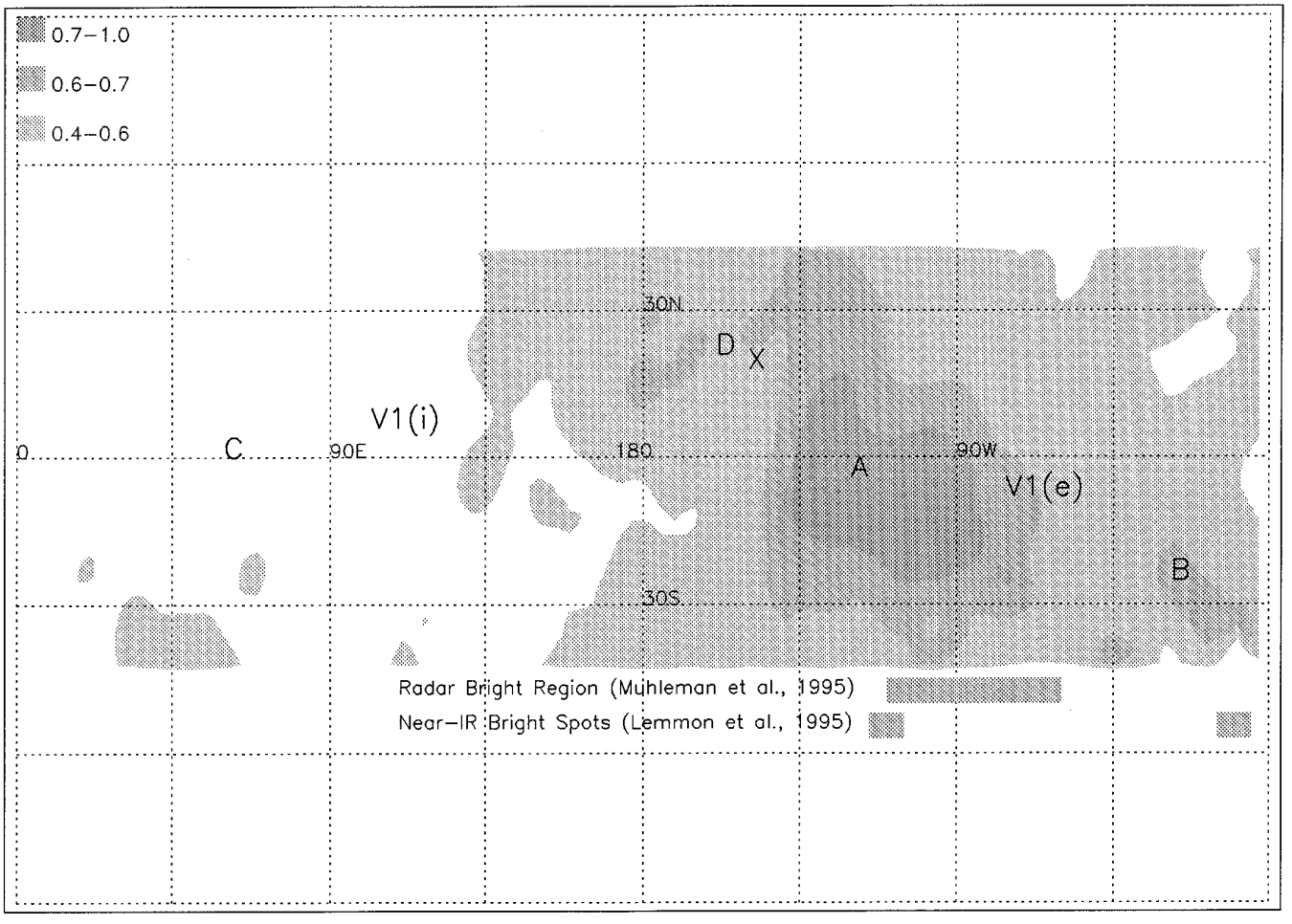

FIG. 8. A schematic map (using the F850LP data from Fig. 4b) indicating the features described in the text and Fig. 3 (A, center of the bright feature; B, small bright region; C, dark region; D, spit), and which shows the location of the Huygens probe entry (X), and the Voyager 1 radio occultation ingress and egress (V1(*i*) and V1(*e*), respectively). Note that this figure has darker shades of gray allocated to the brighter regions, with arbitrary shading thresholds at 0.4, 0.6, and 0.7 times the total surface contrast (i.e., total brightness 3.1, 4.6, and 5.4% above the darkest region). Shaded bars at the base of the map indicate the longitudes of the bright regions seen by ground-based disk-averaged radar and near-IR observations.

cosmic abundances and the current understanding of Titan, in particular the low density of Titan (1.88 g cm^{-3}), suggests that about 50% of its mass is ice. Although Griffith *et al.* (1991) and Lemmon *et al.* (1995) found no evidence for strong water ice absorption features in near-infrared spectra of Titan, the suggestion by Griffith *et al.* of dirty water ice is still viable as the major constituent of the bright surface region, as only small quantities of impurities are required to attenuate the absorption bands.

The first possibility for feature generation implies a recently active surface, since only a small layer of tholin, which continuously falls out of the atmosphere, is required to darken a surface. Specifically, the reflectivity of tholin is about 0.1, and the e^{-1} absorption depth is given by $\sim\lambda/4\pi n_i$, where n_i is the imaginary index of refraction (10^{-3} at 1000 nm, Khare *et al.* 1984), or about 80 μm (compared with ~10 cm for water ice). The deposition rate of acetylene and other solid hydrocarbons produced by atmospheric photochemistry is ~40 m/4.5 Gyr (Lara *et al.* 1994). Hence the formation of a dark coating of a few hundred μm requires only ~30 kyr: the implication is that an impact or volcanic event able to resurface a substantial portion of Titan's surface has occurred very recently. (Note that the ethane deposition rate predicted by the Lara *et al.* (1994) photochemical model is ~200 m/4.5 Gyr. The corresponding hydrocarbon ocean is shallow enough to be nonglobal: see also reviews by Lorenz (1993b) and Lunine (1993).)

Lorenz (1995) suggests that an upper limit on the resurfacing rate due to water–ammonia volcanism could be

derived from heat-flow considerations; if all of Titan's current geothermal heat flow was transported by magma (admittedly an extreme case, but a robust upper limit), the corresponding eruption rate would be 10^{14} kg yr^{-1} (or 10^{11} m^3 yr^{-1}).

Additionally, high (1.5 bar) surface atmospheric pressure and poor solubility of gases in water–ammonia means that cryoclastic eruptions with widespread ash clouds are unlikely: the most probable style of volcanism is effusive. Such eruptions can lead to thick lava flows, and hence large lava volumes. Extrapolating data in Lorenz (1995) suggests that a 1000-km radius lava flow (corresponding in size to the large bright region) would require a lava volume of at least 10^{13} m^3 for even the most fluid (viscosity = 10 Pa sec) water–ammonia magmas. Thus even under the most favorable assumptions, the bright region would require over a century's worth of heat flow to be expressed in a single (or connected group) eruption sometime within the last $\sim 10^4$ years, an improbably cataclysmic event.

The formation rate of craters ($D > 20$ km) on Titan has been computed by Thompson and Sagan (1992) at $\sim 4 \times 10^{-15}$ km^2 yr^{-1}. Assuming a D^{-2} impactor population, an impact large enough to create a 1000-km diameter crater on Titan would be expected only once or twice in the age of the solar system. Even allowing for a smaller (say 200 km) crater associated with a multi-ring basin, and adding volcanism through the associated crustal fissures, the ~30 kyr darkening timescale seems to rule an impact origin out.

The second scenario requires weather to provide steady-state cleansing of the surface, causing brighter terrain at high altitudes. As suggested by Griffith *et al.* (1991) and Lunine (1992), bright features could be due to increased washing of highland terrain by methane rainfall. This mechanism was investigated from a microphysical standpoint by Lorenz (1993a), who found that since rain evaporates in the undersaturated lower atmosphere, the rain mass flux on elevated terrain could be an order of magnitude higher for a 500-m increase in altitude under present-day equatorial conditions. Although the solubility of dark organic material (e.g., ''tholin'') is modest in methane, the solubility of ice in methane is probably lower (see, e.g., Raulin, 1987), so the net effect of rainfall should be to remove dark material from the surface.

Although the brightening of elevated topography seems plausible, the origin of the topography is unknown. It could be due to impact or volcanic events (although such events could have occurred long ago) or tectonic processes. Our low resolution prevents us from discriminating between a massive highland region (like, say, Tharsis on Mars) and a collection of hills with valleys or puddles of darker material between them.

Some limited constraints can be applied to topography from the Voyager 1 radio-occultation experiment. The occultations took place at 6°N, 258°E (ingress) and 8°S, 76°E (egress—Lindal *et al.* 1983). The former location, assuming Titan rotates synchronously, is on the eastern edge (mid-gray on the map, Fig. 8) of the bright feature. The latter is in the middle of the dark region. The ingress and egress profiles were very well matched, and cut-off occurred, presumably due to occultation by Titan's surface, at titanocentric radii of 2575 ± 0.5 km. Thus the edge of the bright feature can be no more than 1 km higher than the center of the dark region.

If the bright feature was associated with topography, the location might seem somewhat anomalous, in that a bulge would be expected to lie near the sub- or anti-Saturn point, holding the body in synchronous rotation due to tidal considerations. There are two scenarios which would allow the observed geometry.

1. The continent is smaller than another bulge near the sub-Saturn point. To achieve tidal lock requires a difference in moments of inertia of $\sim 10^{-8}$ (Greenberg and Weidenschilling 1984—see also Sears *et al.* 1993). This mass asymmetry could be caused by a continent 1 km thick and 100 km in radius. However, the equilibrium hydrostatic figure of Titan would have a mass asymmetry of 10^{-4}, even if Titan has not completely relaxed to its hydrostatic equilibrium figure, a mass asymmetry corresponding to the dimensions of the bright feature (~3000 km) could still be accommodated without itself dominating the moments of inertia, provided its thickness was <10 km. Note that a hydrostatic bulge would not necessarily have a brightness increase due to increased rainfall, since the atmosphere itself responds to the tidal potential (e.g., a 1-km feature, relative to a spherical Titan, is at a lower barometric altitude near the sub- or anti-Saturn point than if, like the bright feature, it were located near Titan's leading or trailing edge; Lorenz 1992).

2. If the ''continent'' is compensated (i.e., its weight is balanced by upthrust from a buoyant ''root'' in the interior) its effects on moments of inertia are small. For typical ices and water/ammonia liquids as the continental and mantle materials, the compensation depth must be 10 to 30 times the height of the continent. Compensation depths of this order do not seem unreasonable for kilometer-scale topography, given that any fluid mantle may be ~300 km below the surface (Stevenson 1992).

In summary, no conclusive statements can be made regarding the topography of the Titan bright region, although the flanks of the feature (labeled light gray in Fig. 8) probably correspond to relief of less than ~1 km relative to the darker terrain. The center of the bright region could have significant elevation, but is probably well below 10 km. We suggest that the bright feature is dominated by water ice. The dark material could be ice contaminated or covered by silicates or organic solids, or it could indicate a significant covering of liquid hydrocarbons (ethane, methane, and

propane). Although the concept of a ''deep, global ocean'' (Lunine *et al.* 1983), which could be the source of the atmospheric methane, is incompatible with the present observations, the notion that large parts of Titan's surface could be covered with liquids is still highly relevant—see reviews by Lunine (1993) and Lorenz (1993b). Although much of the liquid volume suggested by photochemical models could be concealed in a porous regolith (Stevenson 1992, Kossacki and Lorenz 1995), much could accumulate in crater basins, forming lakes (Lorenz 1994, Dermott and Sagan 1995).

CONCLUSION

With 14 F850LP and 8 F1042M Hubble Space Telescope images, we derived relative albedo maps of Titan's surface. Especially remarkable is a large bright feature on Titan's leading face that provides a plausible explanation for the near-infrared lightcurve. The presence of known surface features on a map of Titan raises several important questions. Why is there a bright feature given that dark hydrocarbons are expected to coat the surface? Are the dark areas liquid? Is Titan still an inactive planet, with volcanism or recent large impact? Are weather patterns over a large mountainous continent responsible for eroding dark material?

These images demonstrate the feasibility of imaging Titan's surface through methane windows and open the way for optical imaging from the Cassini Saturn Orbiter spacecraft to map Titan's surface in more detail. Further, they are being used in planning the coverage of Titan's surface by the radar mapper on the Cassini Orbiter, in connection with the present (96-01) redesign of the Cassini orbit tour.

We found that there are no large scale weather systems that we could reliably track to determine wind speeds. Our study allows for small scale, infrequent, optically thin, or somewhat uniform distributions of clouds. We will continue to study these images and future images to determine whether small scale variations may be cloud features.

We note that the entry point of the ESA Huygens probe occurs at an interesting location, (152 ± 11°W, 18.1°N, marked X on Fig. 8) at the edge of the bright feature. As the probe descends by parachute from an altitude of ~170 km, it will drift eastward in the zonal wind field (Flasar *et al.* 1981), perhaps over onto the bright region. We now know that the surface will be clearly visible in the descent imager (DISR) images throughout the descent.

ACKNOWLEDGMENTS

We are grateful for the support of the Space Telescope Science Institute staff, and especially for the invaluable help of Eddie Bergeron. Support for this work was provided by NASA through Grant G0-5508.01-93A from the Space Telescope Science Institute, which is operated by AURA, Inc., under NASA Contract NAS 5-2655. We thank Phil Stooke, Caitlin Griffith, and Bryan Butler for their careful reviews of the paper.

REFERENCES

Caldwell, J., C. C. Cunningham, D. Anthony, H. P. White, E. J. Groth, H. Hasan, K. Noll, P. H. Smith, M. G. Tomasko and H. A. Weaver 1992. Titan: Evidence for seasonal change—A comparison of Hubble Space Telescope and Voyager images, *Icarus* **97,** 1–9.

Cruikshank, D. P., and J. S. Morgan 1980. Titan: Suspected near-infrared variability. *Astrophys. J.* **235,** L53–L54.

Dermott, S. F., and C. Sagan 1995. Tidal effects of disconnected hydrocarbon seas on Titan. *Nature* **374,** 238–240.

Fink, U., and H. P. Larson 1979. The infrared spectra of Uranus, Neptune, and Titan from 0.8 to 2.5 μm. *Astrophys. J.* **233,** 1021–1040.

Flasar, F. M., R. E. Samuelson, and B. J. Conrath 1981. Titan's atmosphere: Temperature and dynamics. *Nature* **292,** 693–698.

Greenberg, R., and S. J. Weidenschilling 1984. How fast do Galilean satellites spin? *Icarus* **58,** 186–196.

Griffith, C. A. 1993. Evidence for surface heterogeneity on Titan. *Nature* **364,** 511–514.

Griffith, C. A., T. Owen, and R. Wagener 1991. Titan's surface and troposphere, investigated with ground-based, near-infrared observations. *Icarus* **93,** 362–378.

Khare, B. N., C. Sagan, E. T. Arakawa, F. Suits, T. A. Callcott, and M. W. Williams 1984. Optical constants of organic tholins produced in a simulated titanian atmosphere: From soft X-ray to microwave frequencies. *Icarus* **60,** 127–137.

Kossacki, K. J., and R. D. Lorenz 1995, Hiding Titan's ocean: Densification and hydrocarbon transport in an icy regolith. *Planet. Space Sci.* submitted.

Lara, L. M., R. D. Lorenz, and R. Rodrigo 1994. Liquids and solids on the surface of Titan: Results of a new photochemical model. *Planet. Space Sci.* **42,** 5–14.

Lemmon, M. T., E. Karkoschka, and M. Tomasko 1995. Titan's rotational lightcurve. *Icarus* **113,** 27–38.

Lemmon, M. T. 1994. *Properties of Titan's Haze and Surface.* Ph.D. Dissertation, University of Arizona.

Lemmon, M. T., E. Karkoschka, and M. Tomasko 1993. Titan's rotation: Surface feature observed. *Icarus* **103,** 329–332.

Lindal, G. F., G. E. Wood, H. B. Hotz, D. N. Sweetnam, V. R. Eshleman, and G. L. Tyler 1983. The atmosphere of Titan: An analysis of the Voyager 1 radio occultation measurements. *Icarus* **53,** 348–363.

Lorenz, R. D. 1995. Pillow lava on Titan: Expectations and constraints on cryovolcanism. *Planet. Space Sci.* in press.

Lorenz, R. D. 1994. Crater lakes on Titan: Rings horseshoes and bullseyes. *Planet. Space Sci.* **42,** 1–4.

Lorenz, R. D. 1993a. The life, death and afterlife of a raindrop on Titan. *Planet. Space Sci.* **41,** 647–655.

Lorenz, R. D. 1993b. The surface of Titan in the context of ESA's Huygens probe. *ESA J.* **17,** 275–292.

Lorenz, R. D. 1992. Gravitational tide in the atmosphere of Titan. In *Proceedings of the Symposium on Titan, Toulouse, France, September 1991. ESA SP-338,* pp. 119–123.

Lunine, J. I. 1993. Does Titan have an ocean? A review of current understanding of Titan's surface. *Rev. Geophys. Space Phys.* **31,** 133–149.

Lunine, J. I. 1992. Plausible surface models for Titan. In *Proceedings of*

the Symposium on Titan, Toulouse, France, September 1991. ESA SP-338, 233–239.

Lunine, J. I., D. J. Stevenson, and Y. L. Yung 1983. Ethane ocean on Titan. *Science* **222,** 1229–1230.

Muhleman, D. O., A. W. Grossman, and B. J. Butler 1995. Radar investigations of Mars, Mercury, and Titan. *Annu. Rev. Earth Planet. Sci.* **23,** 337–374.

Muhleman, D. O., A. W. Grossman, B. J. Butler, and M. A. Slade 1990. Radar reflectivity of Titan. *Science* **248,** 975–980.

Neff, J. S., D. C. Humm, J. T. Bergstrahl, A. L. Cochran, E. S. Barker, and R. G. Tull 1984. Absolute spectrophotometry of Titan, Uranus and Neptune: 3500–10500 Å. *Icarus* **60,** 221–235.

Raulin, F. 1987. Organic chemistry in the oceans of Titan. *Advances in Space Research* **7** (5)71–(5)81.

Saint-pé, O., M. Combes, F. Rigaut, M. Tomasko, and M. Fulchignoni 1993. Demonstration of adaptive optics for resolved imagery of solar system objects: Preliminary results on Pallas and Titan. *Icarus* **105,** 263–270.

Sears, W. D., J. I. Lunine, and R. Greenberg 1993. Equilibrium nonsynchronous rotation of Titan. *Icarus* **105,** 259–262.

Smith, P. H., M. T. Lemmon, J. J. Caldwell, M. D. Allison, and L. A. Sromovsky 1994. HST Imaging of Titan, 1994. *Bull. Am. Astron Soc.* **26,** 1181 [Abstract].

Smith, P. H., and M. Lemmon 1993. HST images of Titan. *Bull. Am. Astron. Soc.* **25,** 1105 [Abstract].

Sromovsky, L. A., V. E. Suomi, J. B. Pollack, R. J. Kraus, S. S. Limaye, T. Owen, H. E. Revercomb, and C. Sagan 1981. Implications of Titan's north-south brightness asymmetry. *Nature* **292,** 698–702.

Stevenson, D. J. 1992. The interior of Titan. In *Proceedings of the Symposium on Titan, Toulouse, France, September 1991.* ESA SP-338, pp. 29–33.

Thompson, W. R. and C. Sagan 1992. Organic chemistry on Titan—Surface interactions. In *Proceedings of the Symposium on Titan, Toulouse, France September 1991.* ESA SP-338, pp. 167–176.